GRAPHICAL PROCEDURE FOR THE EXAMINATION OF TURBO-GENERATORS IN ASYNCHRONOUS OPERATION

By

F. CSÁKI

Department for Special Electric Machines and Automation,
Polytechnical University, Budapest

(Received July 3, 1960)

In the previous *chapters 4, 5* [2] and *6* [3] the advantages and disadvantages in the analytic procedure of the general method suggested in *chapter 3* [1] were shown in details. Turning from the linear approximation to the quadratic one, the analytical procedure has lost much of its simplicity, clearness and perspicuity. Application of the interesting theoretical results obtained becomes difficult in the everyday engineering practice, for, as we have seen, apart from some very special cases calculation of elliptic integrals — moreover laboriously evaluable elliptic integrals of third kind — would be necessary.

7. Graphical construction

For surmounting the above-mentioned practical difficulties, graphical, numerical, or mechanical integration seem to be available.

But if we have to refuse the analytic determination of the function $t(\delta)$ on account of practical considerations, the question arises, whether there is a reason for the analytic calculation of the function $s(\delta)$ at all. The above question arises the more so that function $s(\delta)$ may be expressed simply only in case an equation of second degree in s must be solved at most, while to attain this aim, the direct-axis and quadrature-axis admittance diagrams assumed as being known must be approximated by a straight line, or at most, by a curve of second degree. Then it seems to be more practicable to make immediate use of the direct-axis and quadrature-axis admittance diagrams themselves assumed as being known and to determine relation $s(\delta)$ by a graphical construction.

7.1. Determination of the slip-angle relation by graphical construction

Theoretical principles of the graphical procedure serving to determine the slip-angle relation $s(\delta)$ may already be found in *clause 3.2.*

Starting point of the method suggested (concerning the analytical, as well as the graphical method) is as follows: the terminal-point of the resul-

tant admittance vector $\dot{y}$ (and simultaneously that of the stator current and apparent power vector) is determined by the point of intersection of the straight line $g = \text{const}$ and of the circles C_s plotted for different slips s.

Consequently, by a graphical procedure the relation $s(\delta)$ may be obtained in the following manner : with a suitable choice of slip values (*e.g.* with steps of 10^{-4}) a set of circles must be plotted in such a way that each circle should pass through the corresponding points of the direct-axis and quadrature-axis admittance diagram belonging to the respective slip. For any arbitrary slip value, the corresponding circle C_s intersects the straight line $g = \text{const}$ generally at two points (*see* M' and M'' in Fig. 7—1). Reading by an

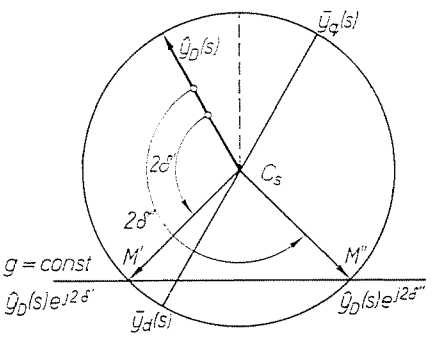

Fig. 7—1

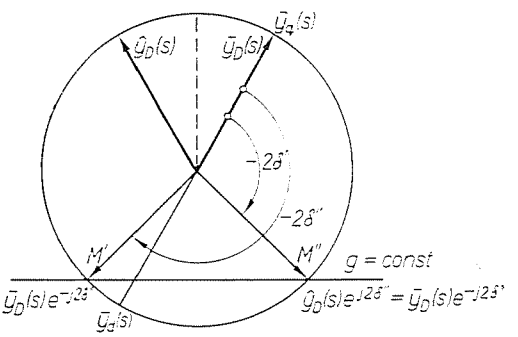

Fig. 7—2

angle meter the angle 2δ included by the radius vector $\hat{y}_D\, e^{j2\delta}$ belonging to the points of intersection and by the initial position of the radius vector $\hat{y}_D$, generally two values, $2\delta'$ and $2\delta''$ may be obtained for the angle. Repeating the above procedure for all circles C_s crossing, or being at least tangential to the straight line $g = \text{const}$ related to the given constant torque, as a result the relation $s(\delta)$ may be evaluated point by point from the slip s and from the angle δ.

It must be noted, that the practical evaluation of the slip-angle function $s(\delta)$ may further be simplified. Namely, it is unnecessary to separately construct the conjugate-complex vector $\hat{y}_D$ in order to render, starting from it, the angle 2δ readable in counter-clockwise sense, but due to the manifest image symmetry about the real axis, it is sufficient to start from the initial position of vector $\bar{y}_D$ determined by the terminal points of the vectors $\bar{y}_q$ and $\bar{y}_d$ being otherwise necessary, too, to read the angle 2δ, advancing in clockwise direction up to the points of intersection (Fig. 7—2). In this way the graphical procedure offers not only greater simplicity, but also higher accuracy. Naturally, care must be taken to interchange the angle values so obtained, for example the angle δ' belongs in reality to the point of intersection M' and not to M''.

7.2. *Further steps of the graphical procedure*

Determining the relation $s(\delta)$ in the above-suggested manner, naturally, the reciprocal functions $1/s(\delta)$ and $-1/s(\delta)$ are known too. From the latter the function $t(\delta)$ has to be determined on the basis of the fundamental formula (3—5) [1] by integral calculus. In lack of other auxiliary devices (*e. g.* planimeter), graphical or numerical integration may be adopted. The most practicable solution is to choose abscissa intervals of equal magnitude (*e. g.* 10°) and to read within these intervals one after the other, the medium ordinates of curve $-1/s(\delta)$. Namely, in this way integration can be reduced to a simple addition and instead of the oblong areas just the ordinates may be summarized to obtain the function $t(\delta)$. After establishing functions $t(\delta)$ and $s(\delta)$ the desired function $s(t)$ is also available and may easily be plotted.

In the course of the analytic procedure, to determine the stator current, functions $\delta(t)$ and $s(t)$ had to be substituted in formula (3—11'). Now the graphical solution gives immediately also the course of the stator current. The distance measured between the point of intersection M' or M'' and the origine O of the co-ordinate system is proportional to the apparent power, that is, to the instantaneous value of the stator current envelope curve. Consequently, the point of intersections provide not only the slip-angle relation, but also the relation between the angle and the apparent power, as well as the stator current. So, after having determined the time-angle relation by integration, also the time course of the stator current may be simply established.

Finally another remark : in the course of the analytic procedure the calculations made use of the resultant admittance vector and its components, as, on the one hand, formulae became more simple and, on the other hand, one single formula gives information about the current and the power (moreover, in certain cases, also about the torque). In connection with the graphical procedure it is needless to return to the admittances, as the current-vector and power-vector diagrams may directly be employed, using either relative units, or defined ones (volt, amper, etc).

7.3. *Application of the measurements data*

In view of the preceding discussion, knowing the direct-axis and quadrature-axis admittance diagram, realizing the procedure of graphical construction encounters no particular difficulties, consequently it represents a simple and quick solution for engineering practice. Unfortunately, due to the complications arising in the practice of measurements, plotting of the amplitude-phase-frequency curves the so-called frequency-response (*Nyquist* curves) customary in control engineering which is dealt with in the field of syn-

chronous machines only since recently [*e.g.* 4], and, on the other hand, because of the solid iron computation of the admittance diagrams is an intricate task, starting besides from several simplifying suppositions. So it is to be understood, that generally no direct-axis and quadrature-axis admittance (or current) diagrams are available.

As a consequence the simple graphical construction outlined in the foregoing, seems to be endangered just in respect to the starting bases.

As determination of the admittance diagrams is always based on measurements, — either the amplitude-phase-frequency characteristics are to be taken directly by measurements, or the parameters figuring in the theoretical calculations are to be cleared up in an indirect way by preliminary measurements — the question arises, whether the results of the measurements themselves carried out in an asynchronous operation could not be applied for determining the section relative to small slips of the direct-axis and quadrature-axis admittance diagrams.

Let it be supposed that corresponding to the same slips two set of circles C_s' and C_s'' of the resultant admittance (or current) are known for two cases : for the directly short-circuited field circuit and for the field circuit closed through the de-exciting resistance. Since the insertion of the de-exciting resistance evidently influences merely the direct-axis admittance (or current) diagram, while the quadrature-axis admittance (or current) diagram remains unchanged, the point of intersection Q_s of the two circles C_s' and C_s'' belonging to arbitrary, but the same slip s (Fig. 7—3) must lie on the quadrature-axis curve, as the given slip s may determine, but a single point on the latter, through which both circles C_s' and C_s'' have to pass. It is worth mentioning that circles C_s' and C_s'' intersect each other at two points, the right-side one being generally the desired point Q_s. Points D_s' and D_s'', however, corresponding diametrically to the above point Q_s within circles C_s' and C_s'' lies on one or the other of the direct-axis admittance, or current diagrams. In this way the quadrature-axis diagram, and then the two direct-axis diagrams sought for may be plotted from the two sets of circles C_s' and C_s''.

Now the question arises in a new form: how can the sets of circles C_s' and C_s'' be constructed on the basis of the measurement results? For that purpose the following practical procedure may be suggested:

Let us plot the maximum and minimum reactive power, respectively, belonging to each constant active power (torque), that is, let us plot the points corresponding to the terminal points of the vectors belonging to the maximum and minimum apparent power (or current) in a co-ordinate system having the active power P on the real axis, while on the imaginary one the reactive power Q. On the basis of the points measured, the limit-curves S_{max} and S_{min} may be plotted (with more or less equalization). These two curves are at the same time the envelope curves of the set of circles C_s. Consequently,

constructing perpendicular lines to the single envelope curves and halving their section extending up to the other curve, the desired geometrical locus C of the centres of the circles C_s may be constructed with a practically adequate accuracy. Curve C must also be provided with a suitable slip calibration. This may be realized by first writing the measured medium slips in the points of intersection of the straight lines $P = \text{const}$ and of the centre curve C, further the callibration has to be rendered more precise by interpolation. In the meantime the uniformity of the slip-scale must be aimed at. Finally the set of circles may be plotted without difficulty, on the basis of the slip-scale on the centre curve and of the two envelope curves.

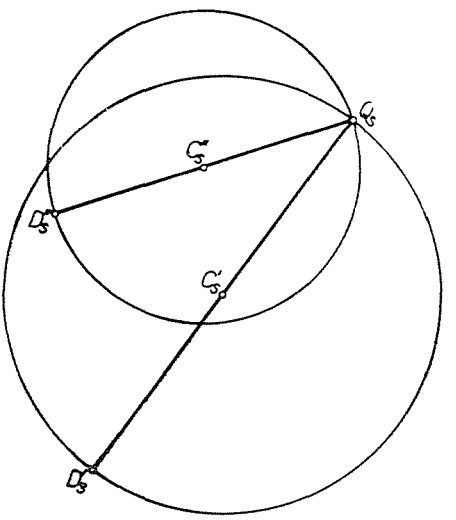

Fig. 7—3

The above-described construction involves several neglections. During asynchronous operation and measurement, not speaking about the voltage, neither the active power, nor the torque is constant in the strict sense of the word, and also the measured medium slip s_m serving as a basis for the slip-scale deviates, though not too much, from the slip value s_0, which would be formed if circles C_s shrank to their centre. Nevertheless, the slip-scale is actually constructed starting from values s_m and not from the true values s_0.

8. Comparison of the theoretical and experimental results

To be able to judge competence, effectiveness and accuracy of the method suggested, the present chapter for some cases compares the curves constructed or calculated on the basis of the method suggested with the curves

Table 8—1/a

Turbo-generator: 26.5 MWA; 10.5 kV; 1460 A; cos $\varphi = 0.75$; 3000 r. p. m.
Bronze slot-wedges

Synchronous operation					
P	MW	3.0	5.1	8.1	12.0
Q	MVAr	4.0	3.3	3.6	6.9
U	kV	11.1	11.2	11.2	11.2
I	kA	0.27	0.35	0.50	0.72
I_f	A	360	360	400	465
Asynchronous operation. Short-circuited field					
P_m	MW	3.0	5.1	8.1	12.4
Q_{max}	MVAr	19.7	22.8	27.6	32.0
Q_{min}	MVAr	15.7	16.5	17.4	18.6
U_{max}	kV	11.1	11.1	11.0	11.1
U_{min}	kV	10.9	10.9	10.8	10.7
I_{max}	kA	1.08	1.25	1.56	1.85
I_{min}	kA	0.86	0.91	1.04	1.17
I_{fmax}	A	72	101	170	230
T_{max}	sec	106	64.4	40.2	27
T_{min}	sec	106	62.2	39.2	26.6
T_m	sec	106.0	63.6	39.6	26.8
s_m	%	0.0189	0.0314	0.0505	0.0746

evaluated from the measurements results. At first the graphical procedure discussed in *chapter 7* will be criticized for four cases, and then judgement of the piecewise-linear approximation, being a version of the analytic procedure dealt with in *chapter 5* will be given.

8.1. Comparison of graphical procedure and measurements

The graphical procedure described in *chapter 7* — to judge its accuracy, expediency and practicability — will be compared with the measurement results. This comparison also serves for judging the suggested method in its entirety: to form an opinion about the starting principles and about the permissibility of the neglections made.

Comparison is based upon the stator-current versus time curves determined by measurement and plotted graphically. Opposite to the current and voltage curves, the direct measurement and oscillograph record of the slip-

Table 8—1/b

Turbo-generator: 26.5 MWA; 10.5 kV; 1460 A; cos $\varphi = 0.75$; 3000 r. p. m.
Bronze slot-wedges

Synchronous operation						
P	MW	3.0	5.4	8.4	12.3	15.3
Q	MVAr	4.0	3.4	3.6	6.3	4.7
U	kV	11.1	11.1	11.2	11.2	11.2
I	kA	0.27	0.36	0.51	0.72	0.85
I_f	A	360	360	380	465	475
Asynchronous operation Field closed through de-excitation resistance						
P_m	MW	3.1	5.4	7.8	11.8	15.3
Q_{max}	MVAr	19.4	21.8	25.2	28.8	32.4
Q_{min}	MVAr	16.0	17.2	18.9	21.0	22.8
U_{max}	kV	11.1	10.9	10.9	11.0	10.9
U_{min}	kV	10.9	10.8	10.8	10.7	10.6
I_{max}	kA	1.05	1.2	1.42	1.67	1.91
I_{min}	kA	0.89	0.99	1.08	1.28	1.44
I_{fmax}	A	29	54	78	101	130
T_{max}	sec	70	33.9	22.6	15.7	11.0
T_{min}	sec	70	33.8	22.0	15.5	10.8
T_m	sec	70	33.8	22.2	15.6	10.8
s_m	%	0.0286	0.0590	0.0900	0.1280	0.1850

time and angle-time curves is not encountered in everyday practice, consequently determination of the latter two curves may be regarded as one of the practical results of the graphical procedure.

As further on the instrument readings may serve merely for the starting basis of the graphical construction and in addition to the angle-time, slip-time curves also the stator current can be simply established, the graphical procedure may ever supersede application of the electromagnetic oscillograph, or may replace it in certain cases.

8.2. Measurement results

The measurement results serving for the starting point may be found in Tables 8—1 and 8—2, referring to 26 MVA turbo-generators, on the rotor with bronze and steel slot-wedges, respectively, for the cases of a directly short-circuited field and through a de-excitation resistance closed one.

Table 8—2/a

Turbo-generator: 26.5 MWA; 10.5 kV; 1460 A; cos $\varphi = 0.75$; 3000 r. p. m.
Steel slot-wedges

Synchronous operation						
P	MW	3.0	5.6	9.0	12.3	15.0
Q	MVAr	2.4	1.8	1.1	4.8	5.3
U	kV	11.1	11.1	11.1	11.2	11.2
I	kA	0.24	0.35	0.48	0.68	0.84
I_f	A	330	320	340	430	480
Asynchronous operation. Short-circuited field						
P_m	MW	3.0	5.3	8.7	13.5 11.5	15.6 13.2
Q_{max}	MVAr	18.0	21.2	26.7	31.2	36.0
Q_{min}	MVAr	15.0	15.4	16.9	18.8	20.4
U_{max}	kV	10.7	10.7	10.7	10.6	10.5
U_{min}	kV	10.6	10.5	10.4	10.3	10.3
I_{max}	kA	1.10	1.20	1.60	1.90	2.14
I_{min}	kA	0.83	0.90	1.09	1.23	1.36
I_{fmax}	A	72	110	180	240	280
T_{max}	sec				18.3	13.8
T_{min}	sec				17.6	13.4
T_m	sec	86.6	47.4	26.4	18.0	13.6
s_m	%	0.0231	0.042	0.076	0.111	0.147

In Fig. 8—1 the oscillogram of a test made with directly short-circuited field coil referring to the 8.1 MW loading of the generator with bronze slot-wedges on the rotor may be seen (8 MW BO), while Fig. 8—2 shows the oscillogram of the measurement made on the same machine loaded by 12.3 MW with insertion of the de-excitation resistance (12 MW BR). Fig. 8—3 illustrates the oscillogram of the test referring to a generator with steel-wedge rotor-slots, loaded by 12.3 MW, with directly short-circuited field coil (12 MW AO), finally in Fig. 8—4 the oscillogram referring to a 15.2 MW loading and to a field coil closed through the de-excitation resistance (15 MW AR) may be seen.

8.3. Details of the graphical procedure

In Figs. 8—5 and 8—6 construction of the sets of circles referring to the turbo-generator with bronze slot-wedges on the rotor, in Figs. 8—7 and 8—8

Table 8—2/b

Turbo-generator: 26.5 MWA; 10.5 kV; 1460 A; cos $\varphi = 0.75$; 3000 r. p. m.
Steel slot-wedges

Synchronous operation

P	MW	3.3	5.6	8.8	12.2	15.1	17.4
Q	MVAr	0.6	1.0	1.5	3.4	5.3	3.2
U	kV	11.1	11.1	11.1	11.1	11.2	11.1
I	kA	0.24	0.33	0.46	0.66	0.84	0.93
I_f	A	290	310	340	410	470	470

Asynchronous operation
Field closed through de-excitation resistance

P_m	MW	3.0	5.0	8.2	14 11.5	16 13.5	19 14.5
Q_{max}	MVAr	17.1	19.5	22.4	27.3	30.6	35.0
Q_{min}	MVAr	15.0	16.2	17.7	20.4	22.2	24.9
U_{max}	kV	10.9	10.9	10.7	10.4	10.6	10.5
U_{min}	kV	10.8	10.7	10.5	10.2	10.3	10.2
I_{max}	kA	0.98	1,18	1.32	1.65	1.89	2.08
I_{min}	kA	0.85	1.00	1.08	1.30	1.50	1.62
I_{fmax}	A	35	50	70	120	140	170
T_{max}	sec		31.6	18.3	11.0	8.27	6.24
T_{min}	sec		26.7	17.6	10.4	8.0	6.02
T_m	sec	48.8	29.2	18.0	10.9	8.24	6.16
s_m	%	0.041	0.068	0.111	0.183	0.243	0.325

that concerning the turbo-generator with steel slot-wedges on the rotor may be seen. Figs. 8—5 and 8—7 refer to the directly short-circuited field, while Figs. 8—6 and 8—8 to the field coil closed through the de-excitation resistance.

In all figures the points marked by a cross designate the measurement data of Tables 8—1 and 8—2, respectively, in the co-ordinate system P, Q, while S_{max} and S_{min} mean the two envelope curves and C the locus of the centres. On the latter the slip-scale is calibrated in 10^{-4} (*i.e.* 0.01 %) steps. Each scale point is simultaneously a centre of a circle.

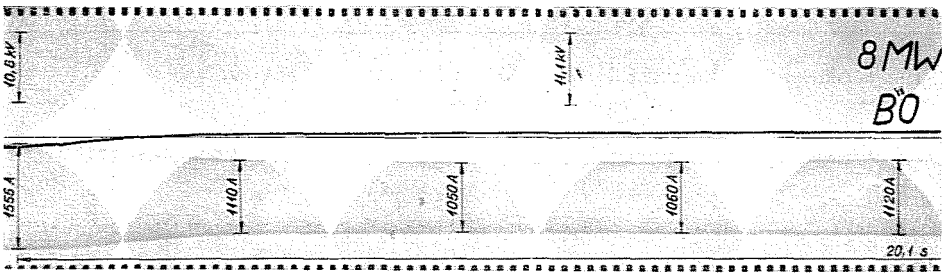

Fig. 8—1/a

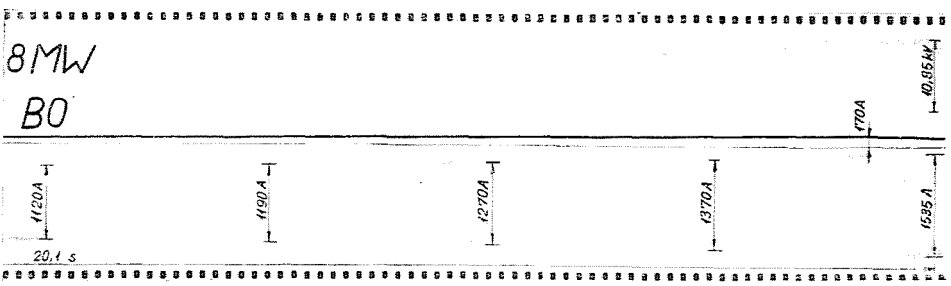

Fig. 8—1/b

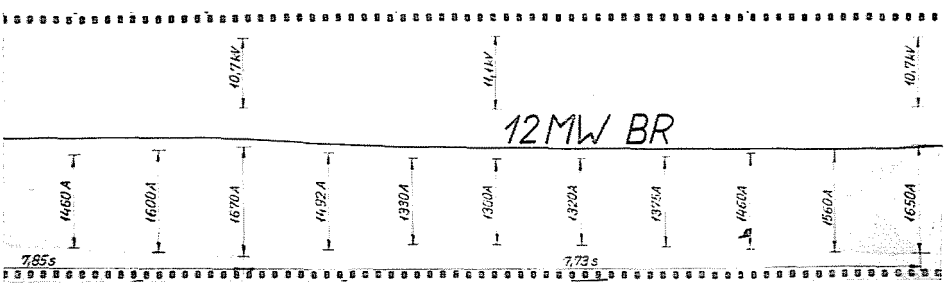

Fig. 8—2

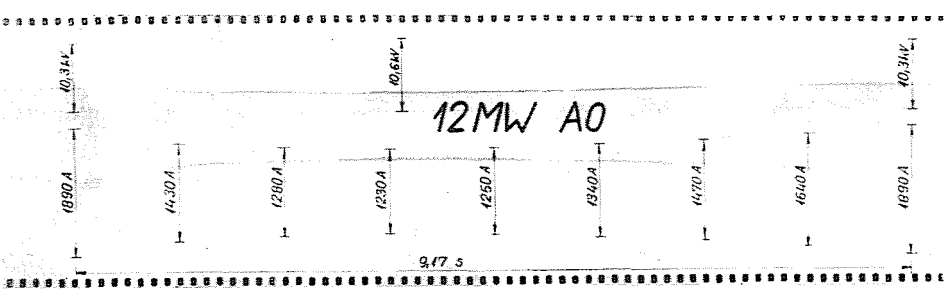

Fig. 8—3

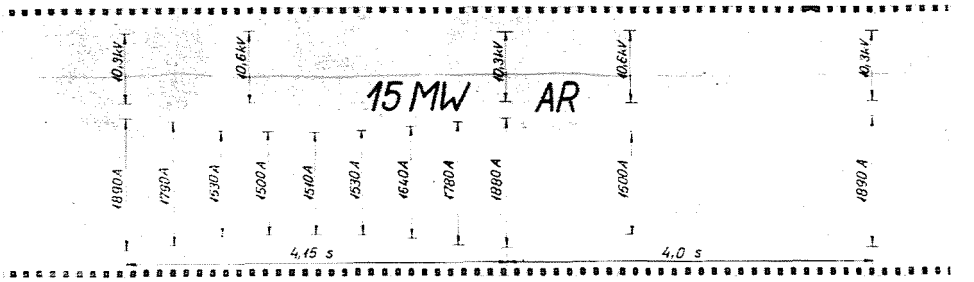

Fig. 8—4

Overlapping the two sets of circles of the bronze-wedge machine (Figs. 8—5 and 8—6) in such way that the co-ordinate axes cover each other, the intersection of the circles belonging to the same slip, as well as the other terminal points of the diameters may be determined. Consequently, the circle diameters providing the necessary starting directions are available (thin lines) and the angle may be measured in the clockwise direction according to Fig. 7—2, merely the intersection points of the straight lines $P = 8.1$ MW and $P = 12.3$ MW, respectively, are to be constructed. A quite similar procedure is to be adopted with the two sets of circles of the turbo-generator with steel slot-wedges on the rotor (Figs. 8—7 and 8—8), nevertheless, now the straight lines $P = 12.3$ MW and $P = 15.2$ MW, respectively, are employed.

The related values of slip s angle δ and current I to be obtained on the basis of the construction are shown in Table 8—3 referring to the bronze-wedge generator with short-circuited field coil, in Table 8—4 referring to the bronze-wedge machine with a field circuit closed through a de-excitation resistance.

Table 8—3

Corresponding values read from Fig. 8—5
(8 MW BO)

$-s$	$-\frac{1}{s}$	$2\delta'$	$2\delta''$	I'	I''
10^{-4}	10^3	°	°	kA	kA
3,5	2.86	169°	205°	1.084	1.17
4	2.5	133°	242.5°	1.04	1.285
5	2.0	101°	280.5°	1.044	1.4
6	1.66	81°	307°	1.09	1.485
7	1.429	62.5°	329.5°	1.166	1.525
8	1.25	40°	355°	1.300	1.515

Scale factors: $\frac{19.25 \text{ cm}}{1.04 \text{ kA}} = 1.85 \text{ cm/kA}$

$\frac{28.85 \text{ cm}}{1.56 \text{ kA}} = 1.83 \text{ cm/kA}$

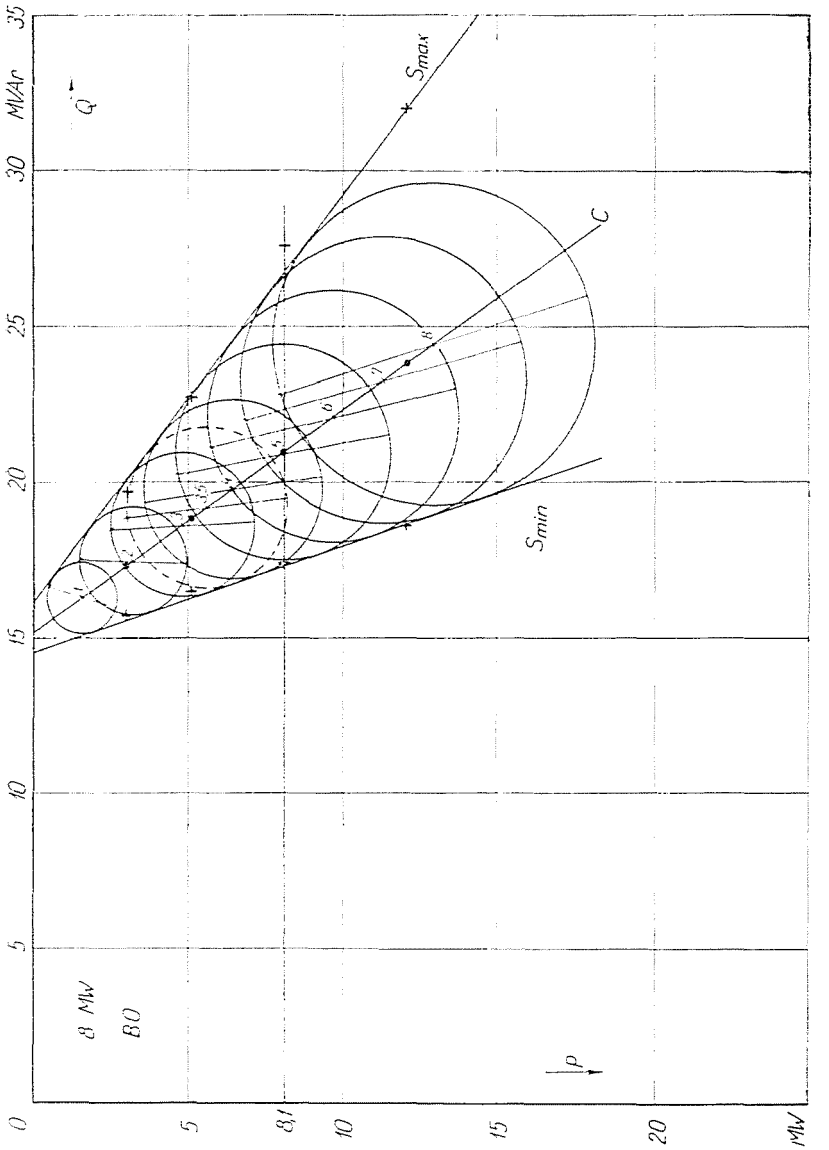

Fig. 8—5

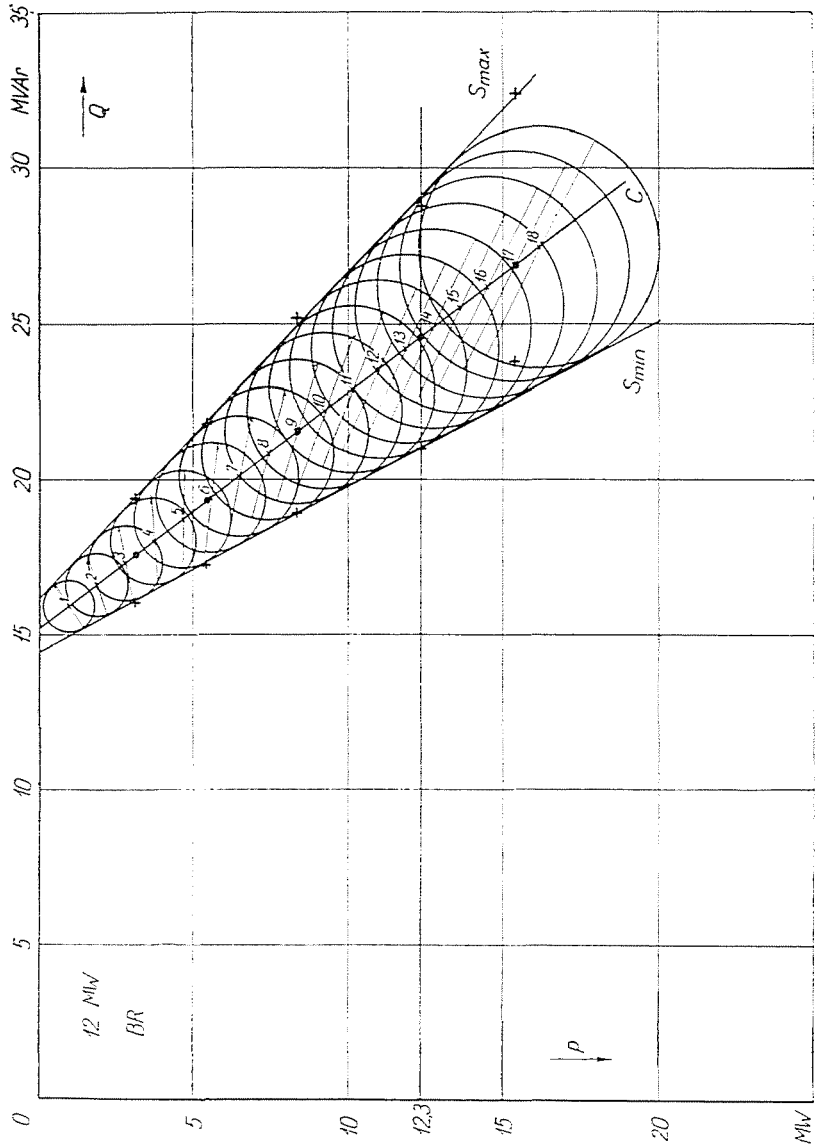

Fig. 8—6

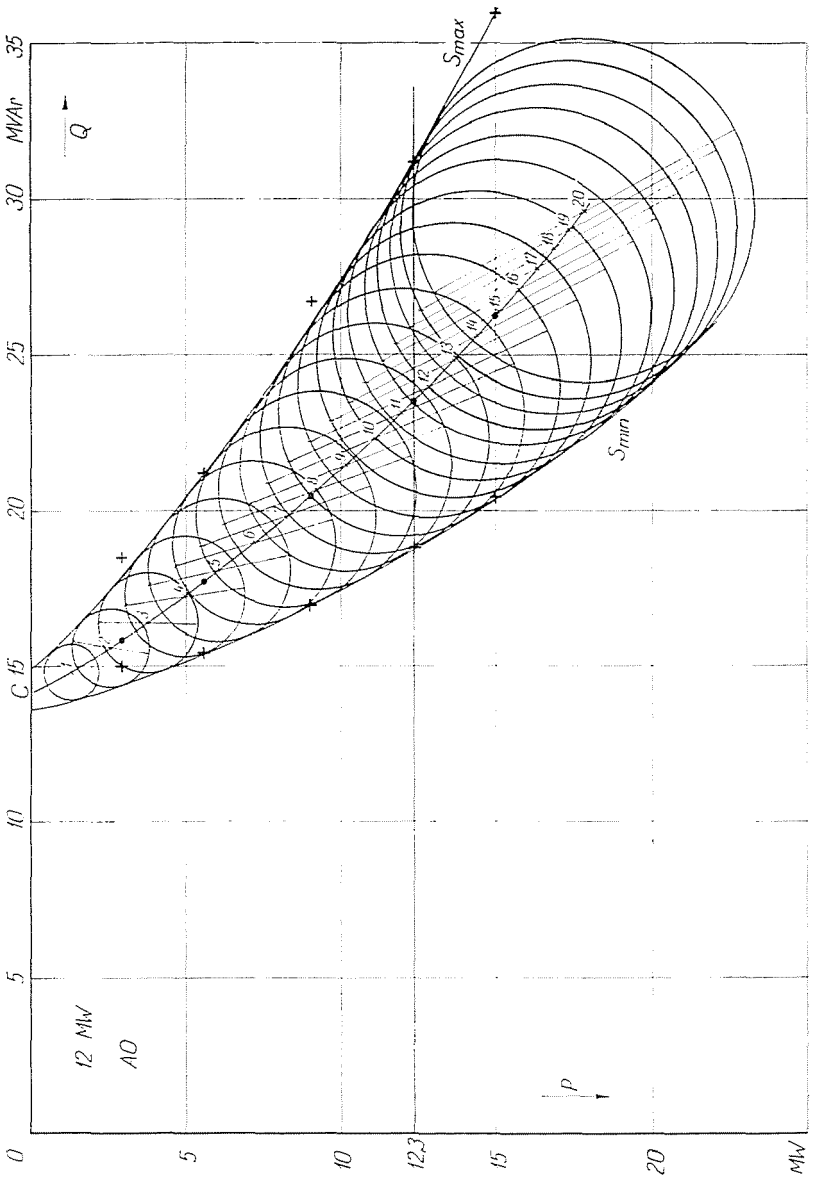

Fig. 8—7

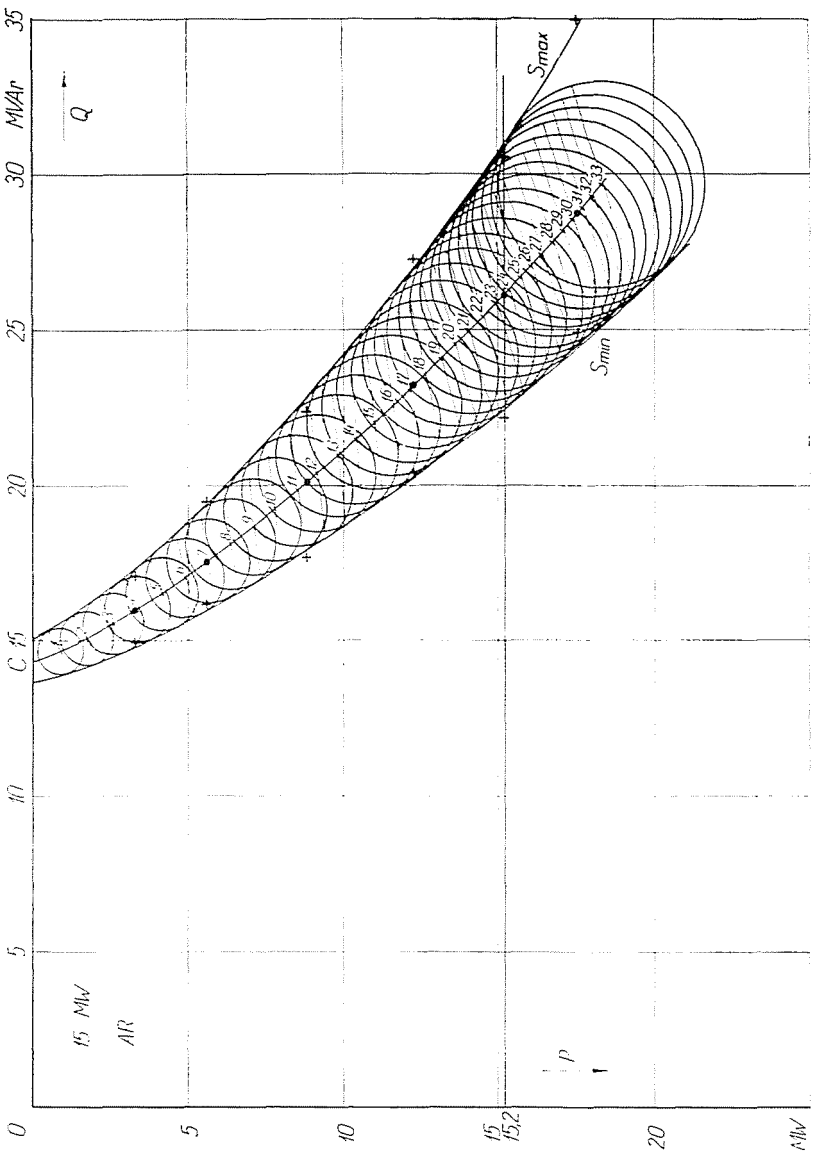

Fig. 8—8

in Table 8—5 relative to the steel-wedge machine of short-circuited field and in Table 8—6 for a steel-wedge generator with a field closed through a de-excitation resistance. It must be noted that when recalculating to kA the currents from the lengths read, the small change in the scale due to the voltage variation was also considered.

Table 8—4

Corresponding values read from Fig. 8—6
(12 MW BR)

$-s$ 10^{-4}	$-\frac{1}{s}$ 10^3	$2\delta'$ °	$2\delta''$ °	I' kA	I'' kA
11	0.909	35.7°	103°	1.325	1.455
12	0.833	3.2°	128°	1.31	1.525
13	0.769	344°	147°	1.315	1.575
14	0.714	328°	162.5°	1.34	1.61
15	0.666	312°	177.4°	1.37	1.635
16	0.625	296°	191.8°	1.41	1.655
17	0.589	278°	209.5°	1.47	1.65
18	0.556	250°	238°	1.57	1.61

Scale factors : $\frac{31.4 \text{ cm}}{1.685 \text{ kA}} = 1.865 \text{ cm/kA}$

$\frac{24.4 \text{ cm}}{1.28 \text{ kA}} = 1.905 \text{ cm/kA}$

For the bronze-wedge machine of short-circuited field coil the curve $-1/s(\delta)$ (see Fig. 8—9) may be plotted on the basis of Table 8—3. Details of its numerical integration may be found in Table 8—7. The coherent values

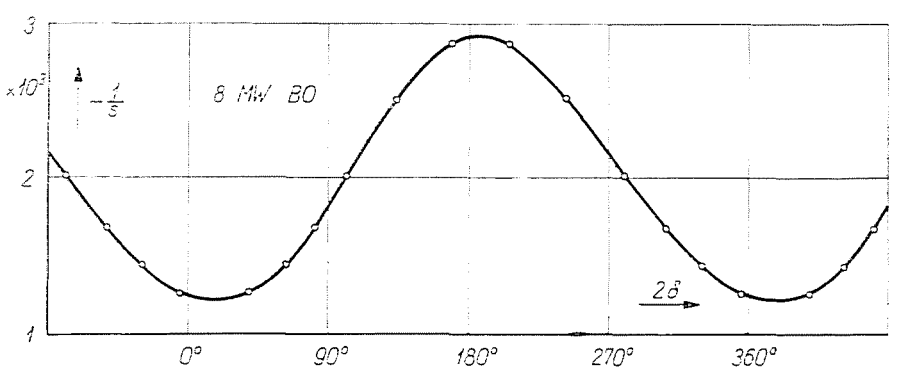

Fig. 8—9

Table 8—5

Corresponding values read from Fig. 8—7
(12 MW AO)

$-s$	$-\frac{1}{s}$	$2\delta'$	$2\delta''$	I'	I''
10^{-4}	10^3	°	°	kA	kA
8	1.25	189°	211°	1.29	1.35
9	1.11	152°	252°	1.23	1.492
10	1.0	133°	273°	1.23	1.583
11	0.909	119°	288°	1.25	1.653
12	0.833	108.5°	302°	1.28	1.714
13	0.769	99°	313°	1.32	1.76
14	0.714	92°	324°	1.36	1.803
15	0.666	83°	332.5°	1.405	1.836
16	0.625	76°	342°	1.46	1.858
17	0.588	68°	349°	1.51	1.874
18	0.555	60°	357°	1.57	1.88
19	0.526	52°	5°	1.642	1.88
20	0.500	37°	21°	1.745	1.84

Scale factors: $\frac{22.60 \text{ cm}}{1.23 \text{ kA}} = 1.836 \text{ cm/kA}$

$\frac{33.73 \text{ cm}}{1.88 \text{ kA}} = 1.794 \text{ cm/kA}$

of Table 8—7 give the desired time-angle relation $t(\delta)$, (Fig. 8—10) and the inverse angle-time relation $\delta(t)$, respectively. On the basis of the latter curve $\delta(t)$ and the relation $s(\delta)$ in Table 8—3, the wanted slip-time function $s(t)$ may now be easily determined (Fig. 8—11). Finally, by reason of curve $t(\delta)$ in Fig. 8—10 and of the relation $I(\delta)$ in Table 8—3, the stator-current versus time relation $I(t)$ sought for may also be plotted (Fig. 8—12). In the same figure the current curve plotted on the basis of the oscillogram shown in Fig. 8—1 is illustrated by a dotted line. (The time of maxima on the curves is chosen arbitrary to coincide, no data being available as regards the actual angular displacement.)

Referring to the turbo-generator with bronze wedges and the field closed through the de-excitation resistance, the negative reciprocal function $-1/s(\delta)$ of the slip-angle relation may be seen in Fig. 8—13, further the curves $t(\delta)$ and $\delta(t)$, respectively, in Fig. 8—14, while the slip-time relation $s(t)$ in Fig. 8—15. Details of the numerical integration itself are summarized in Table 8—8. Finally the current curves $I(t)$ are compared in Fig. 8—16 (the full line

Table 8—6

Corresponding values read from Fig. 8—8
(15 MW AR)

$-s$ 10^4	$-\frac{1}{s}$ 10^3	$2\delta'$ °	$2\delta''$ °	I' kA	I'' kA
18	0.555	(105°)	(105°)	(1.56)	(1,56)
19	0.526	67°	144°	1.51	1.64
20	0.500	51°	159°	1.50	1.69
21	0.476	39°	172°	1.51	1.73
22	0.454	30°	182.5°	1.52	1.755
23	0.435	20°	192°	1.53	1.785
24	0.417	12.6°	200.6°	1.55	1.81
25	0.400	5°	209°	1.57	1.83
26	0.385	359°	216°	1.587	1.845
27	0.371	352.5°	223°	1.594	1.86
28	0.357	346°	231°	1.63	1.868
29	0.345	339°	236°	1.655	1.88
30	0.333	332.5°	243°	1.684	1.888
31	0.323	323°	251°	1.717	1.89
32	0.313	314°	261°	1.758	1.882
33	0.303	303°	272°	1.8	1.873

Scale factors: $\frac{27.16 \text{ cm}}{1.50 \text{ kA}} = 1.81 \text{ cm/kA}$

$\frac{34.50 \text{ cm}}{1.89 \text{ kA}} = 1.825 \text{ cm/kA}$

again marking the constructed current curve, while the dotted one is the measured current curve).

Details of the graphical procedure referring to the turbo-generator with steel-wedge rotor-slots and directly short-circuited field coil (and of the field closed through a de-excitation resistance, respectively) are illustrated in the following figures. The negative reciprocal of the slip-time function: $-1/s(\delta)$ may be seen in Fig. 8—17 (and 8—21, respectively); the time-angle relation $t(\delta)$ and the inverse relation $\delta(t)$ are shown in Fig. 8—18 (and 8—22 respectively); the slip-time curve $s(t)$ is given in Fig. 8—19 (and 8—23, respectively). The corresponding steps of the numerical integration are illustrated in Table 8—9 (and 8—10, respectively). Finally, the current-curves $I(t)$ are compared in Fig. 8—20 (and 8—24, respectively).

Table 8—7

Steps of the numerical integral calculus

(8 MW BO) $1/C = 2 \cdot 0.5 \cdot 10^3 \, \pi/180°$

$\delta°$	$-C\int_0^{\delta}\frac{1}{s}\,d\delta$	$\frac{2}{T}t$	$\delta°$	$-C\int_0^{\delta}\frac{1}{s}\,d\delta$	$\frac{2}{T}t$
0°	0.00	0.0000	180°	172.32	0.4740
	6.12			14.57	
10°	6.12	0.0168	190°	186.89	0.5140
	6.09			14.52	
20°	12.21	0.0336	200°	201.41	0.5540
	6.12			14.22	
30°	18.33	0.0505	210°	215.63	0.5930
	6.20			13.90	
40°	24.53	0.0675	220°	229.53	0.6310
	6.40			13.46	
50°	30.93	0.0850	230°	242.99	0.6685
	6.74			12.93	
60°	37.67	0.1040	240°	255.92	0.7035
	7.25			12.35	
70°	44.92	0.1235	250°	268.27	0.7385
	7.85			11.70	
80°	52.77	0.1455	260°	279.97	0.7705
	8.60			11.08	
90°	61.37	0.1680	270°	291.05	0.8010
	9.40			10.39	
100°	70.77	0.1950	280°	301.44	0.8295
	10.30			9.66	
110°	81.07	0.2230	290°	311.10	0.8550
	11.12			9.02	
120°	92.19	0.2540	300°	320.12	0.8810
	11.90			8.40	
130°	104.09	0.2865	310°	328.52	0.9045
	12.62			7.82	
140°	116.71	0.3210	320°	336.34	0.9260
	13.25			7.34	
150°	129.96	0.3575	330°	343.68	0.9450
	13.75			6.88	
160°	143.71	0.3955	340°	350.56	0.9640
	14.17			6.54	
170°	157.88	0.4345	350°	357.10	0.9825
	14.44			6.26	
180°	172.32	0.4740	360°	363.36	1.0000

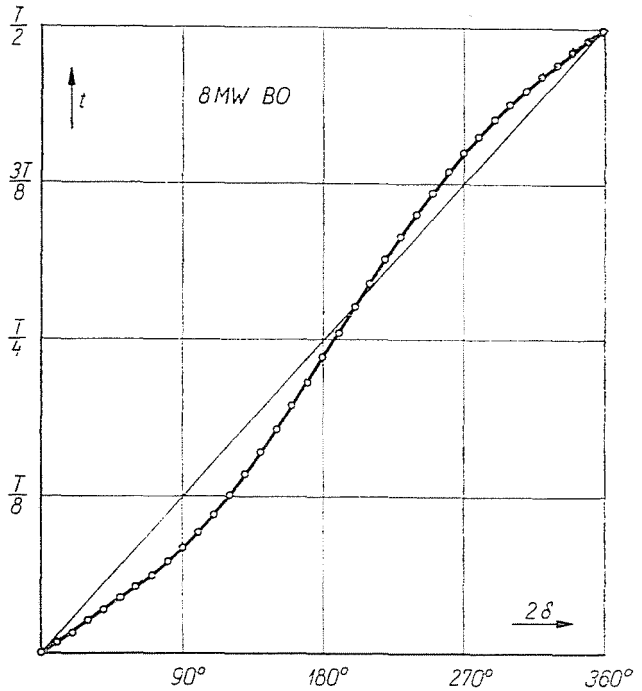

Fig. 8—10

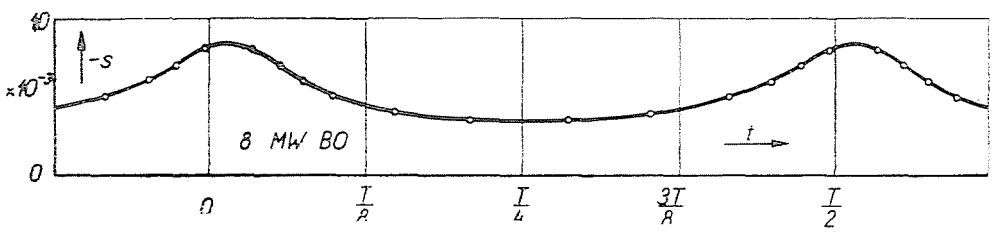

Fig. 8—11

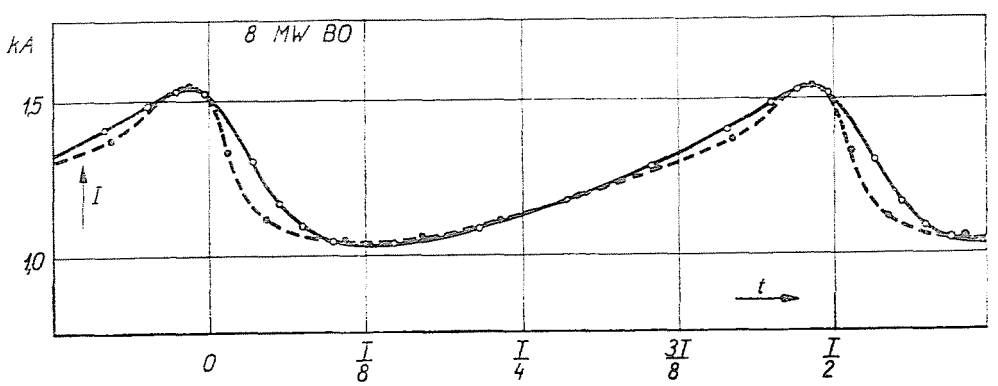

Fig. 8—12

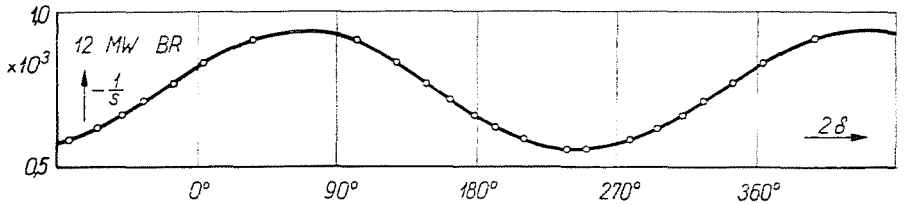

Fig. 8—13

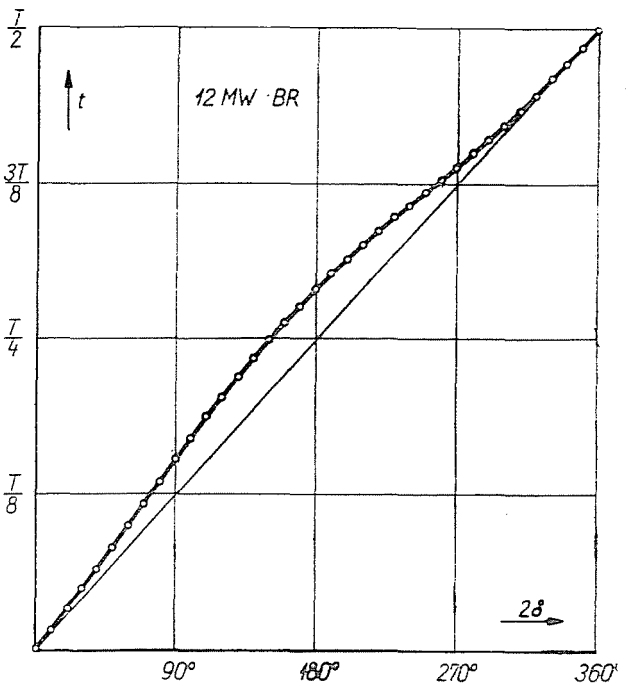

Fig. 8—14

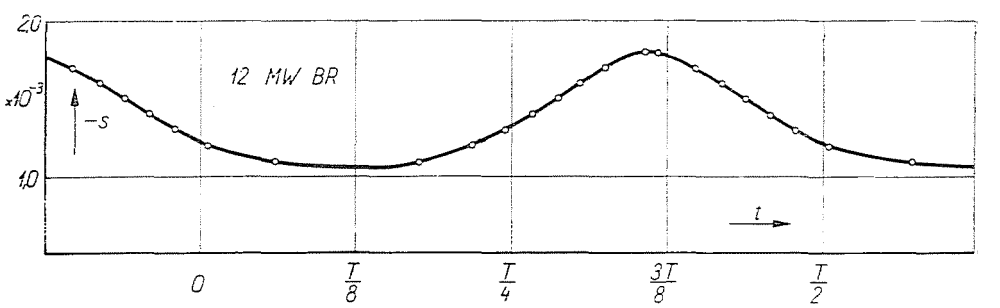

Fig. 8—15

Table 8—8

Steps of the numerical integral calculus

(12 MW BR) $1/C = 0.5 \cdot 10^3\ \pi/180°$

$\delta°$	$-C\int_0^{\delta}\frac{1}{s}\,d\delta$	$\frac{2}{T}t$	$\delta°$	$-C\int_0^{\delta}\frac{1}{s}\,d\delta$	$\frac{2}{T}t$
0°	0.00	0.0000	180°	154.57	0.5815
	8.40			6.44	
10°	8.40	0.0314	190°	161.01	0.6060
	8.67			6.19	
20°	17.07	0.0662	200°	167.20	0.6285
	8.90			5.99	
30°	25.97	0.0970	210°	173.19	0.6515
	9.10			5.83	
40°	35.07	0.1310	220°	179.02	0.6730
	9.25			5.66	
50°	44.32	0.1655	230°	184.68	0.6940
	9.36			5.58	
60°	53.68	0.2007	240°	190.26	0.7150
	9.42			5.54	
70°	63.10	0.2357	250°	195.80	0.7360
	9.42			5.60	
80°	72.52	0.2710	260°	201.40	0.7570
	9.36			5.68	
90°	81.88	0.3060	270°	207.08	0.7780
	9.24			5.83	
100°	91.12	0.3405	280°	212.91	0.7995
	9.05			6.00	
110°	100.17	0.3775	290°	218.91	0.8220
	8.78			6.20	
120°	108.95	0.4070	300°	225.11	0.8450
	8.48			6.45	
130°	117.43	0.4395	310°	231.56	0.8700
	8.12			6.74	
140°	125.55	0.4690	320°	238.30	0.8940
	7.77			7.10	
150°	133.32	0.4980	330°	245.40	0.9210
	7.42			6.43	
160°	140.74	0.5260	340°	251.83	0.9450
	7.08			6.75	
170°	147.82	0.5520	350°	258.58	0.9700
	6.75			8.10	
180°	154.57	0.5815	360°	266.68	1.0000

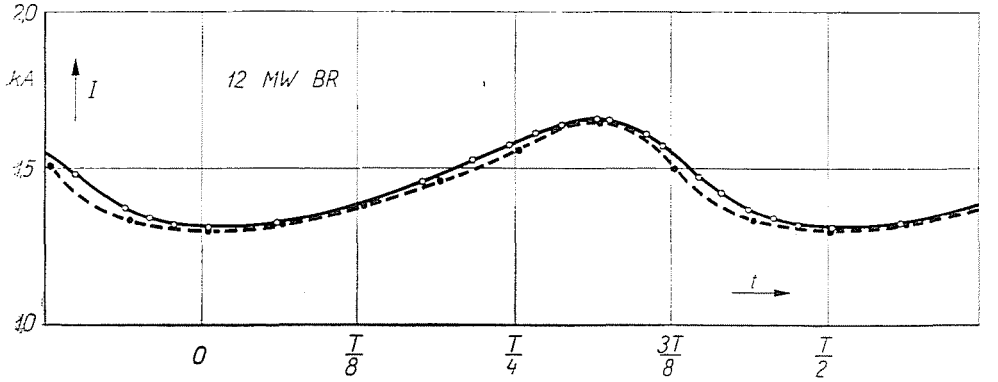

Fig. 8—16

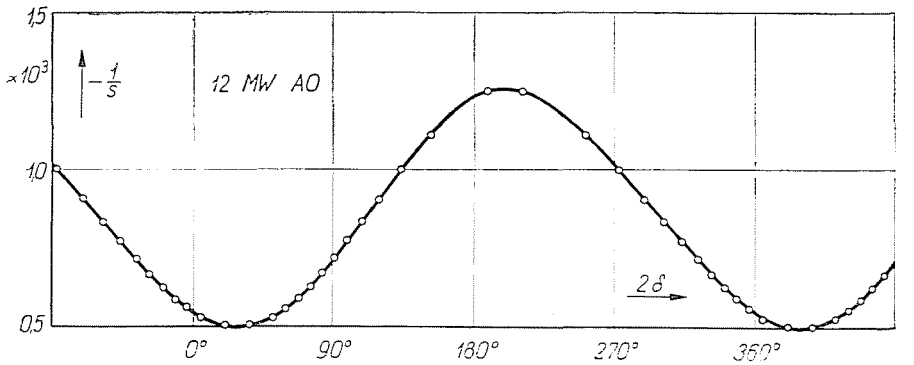

Fig. 8—17

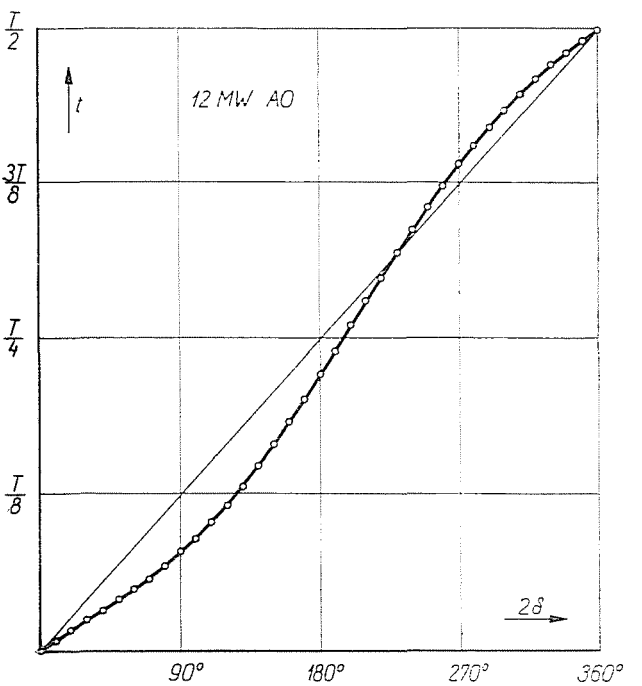

Fig. 8—18

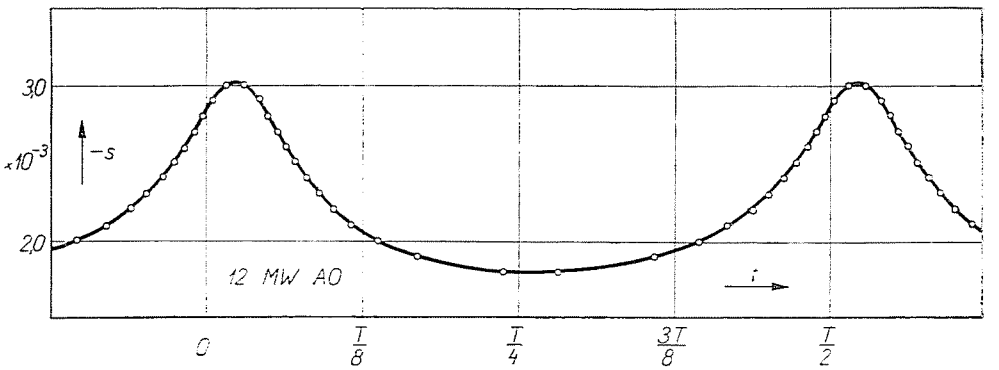

Fig. 8—19

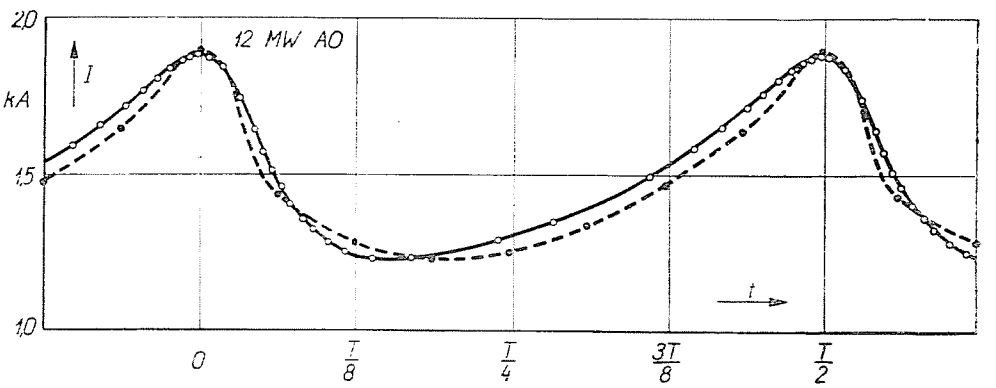

Fig. 8—20

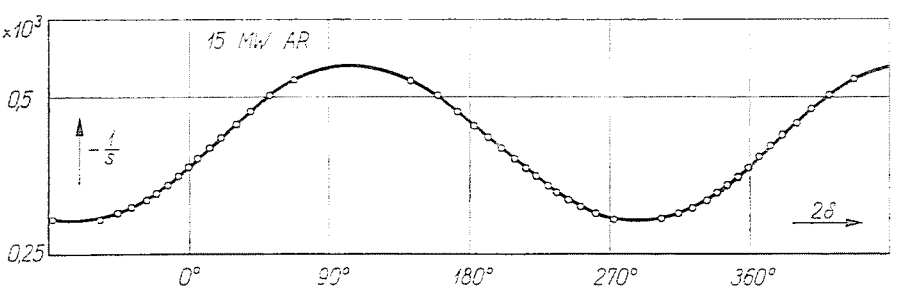

Fig. 8—21

Table 8—9

Steps of the numerical integral calculus

(12 MW AO) $1/C = 0.5 \cdot 10^3 \ \pi/180°$

$\delta°$	$-C\int_0^{\delta}\frac{1}{s}d\delta$	$\frac{2}{T}t$	$\delta°$	$-C\int_0^{\delta}\frac{1}{s}d\delta$	$\frac{2}{T}t$
0°	0.00	0.0000	180°	139.42	0.4425
	5.23			12.45	
10°	5.23	0.0165	190°	151.87	0.4815
	5.07			12.58	
20°	10.30	0.0325	200°	164.45	0.5215
	4.99			12.57	
30°	15.29	0.0485	210°	177.02	0.5610
	5.02			12.43	
40°	20.31	0.0645	220°	189.45	0.6005
	5.11			12.20	
50°	25.42	0.0805	230°	201.65	0.6390
	5.34			11.80	
60°	30.76	0.0975	240°	213.45	0.6760
	5.71			11.47	
70°	36.47	0.1160	250°	224.92	0.7135
	6.20			10.96	
80°	42.67	0.1355	260°	235.88	0.7470
	6.80			10.47	
90°	49.47	0.1570	270°	246.35	0.7815
	7.35			9.81	
100°	56.82	0.1800	280°	256.16	0.8130
	8.14			9.36	
110°	64.96	0.2060	290°	265.52	0.8415
	8.79			8.76	
120°	73.75	0.2340	300°	274.28	0.8700
	9.45			8.20	
130°	83.20	0.2640	310°	282.48	0.8950
	10.13			7.62	
140°	93.33	0.2960	320°	290.10	0.9200
	10.74			7.09	
150°	104.07	0.3300	330°	297.19	0.9355
	11.30			6.49	
160°	115.37	0.3660	340°	303.68	0.9630
	11.87			6.02	
170°	127.24	0.4035	350°	309.70	0.9815
	12.18			5.61	
180°	139.42	0.4425	360°	315.31	1.0000

Table 8—10

Steps of the numerical integral calculus

(15 MW AR) $1/C = 0.5 \cdot 0.5 \cdot 10^3 \, \pi/180°$

$\delta°$	$-C\int_0^{\delta}\frac{1}{s}\,d\delta$	$\frac{2}{T}t$	$\delta°$	$-C\int_0^{\delta}\frac{1}{s}\,d\delta$	$\frac{2}{T}t$
0°	0.00	0.0000	180°	180.80	0.5905
	8.00			8.97	
10°	8.00	0.0261	190°	189.77	0.6200
	8.45			8.57	
20°	16.45	0.0540	200°	198.34	0.6480
	8.89			8.15	
30°	25.34	0.0825	210°	206.49	0.6750
	9.35			7.75	
40°	34.69	0.1135	220°	214.24	0.7000
	9.80			7.35	
50°	44.49	0.1455	230°	221.59	0.7240
	10.16			6.96	
60°	54.65	0.1790	240°	228.55	0.7470
	10.46			6.64	
70°	65.11	0.2130	250°	235.19	0.7690
	10.67			6.34	
80°	75.78	0.2480	260°	241.53	0.7890
	10.83			6.16	
90°	86.61	0.2830	270°	247.69	0.8095
	10.94			6.05	
100°	97.55	0.3195	280°	253.74	0.8285
	10.99			6.01	
110°	108.54	0.3550	290°	259.75	0.8490
	10.94			6.01	
120°	119.48	0.3915	300°	265.76	0.8685
	10.85			6.09	
130°	130.33	0.4265	310°	271.85	0.8880
	10.69			6.25	
140°	141.02	0.4605	320°	278.10	0.9090
	10.47			6.49	
150°	151.49	0.4950	330°	284.59	0.9300
	10.16			6.76	
160°	161.65	0.5285	340°	291.35	0.9515
	9.80			7.12	
170°	171.45	0.5600	350°	298.47	0.9750
	9.35			7.52	
180°	180.80	0.5905	360°	305.99	1.0000

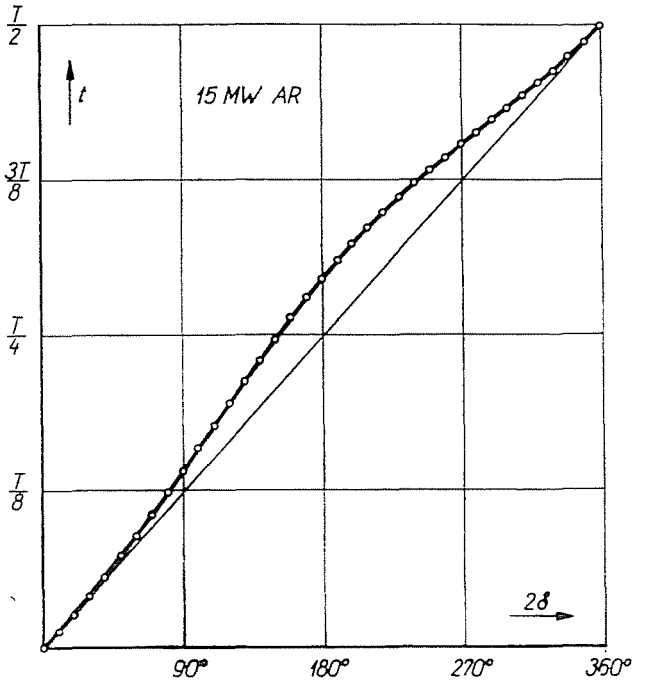

Fig. 8—22

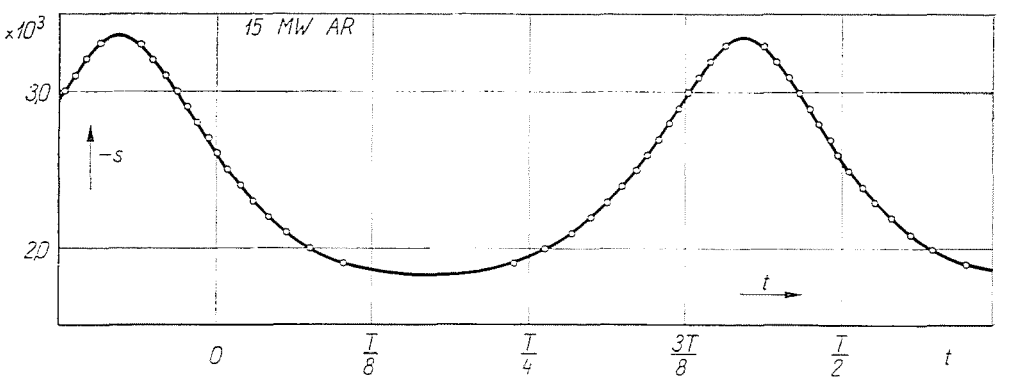

Fig. 8—23

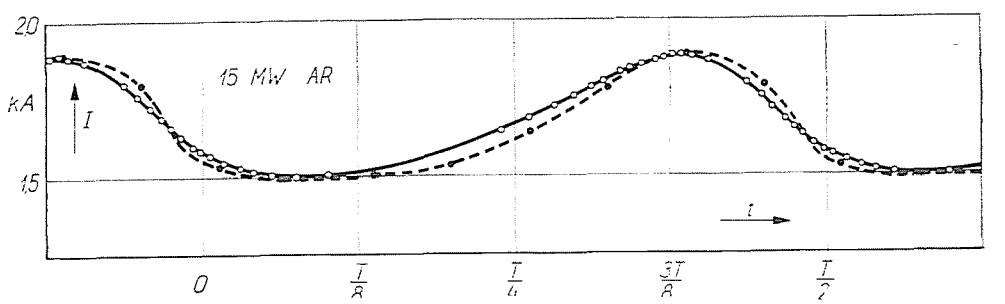

Fig. 8—24

8.4. *Accuracy of the graphical procedure*

As already proved in the preceding discussion, the graphical procedure is not only simple, for in spite of the great number of approximations and neglections it offers a suitable accuracy, as the deviations are permissible in the practice. The constructed and measured current curves almost overlap, their difference being unimportant. Also the fact must be considered that it is not worth while to aim at a higher accuracy, as deviations even in the periods of the measured current curves may be observed. (*See* Figs. 8—1 . . . 8—4.)

A similar statement may be made as regards the slips. The value of the measured medium slip serving for starting basis and the value determined by the graphical procedure — as shown in Table 8—11 — does not deviate from each other even in the most unfavourable case, more than by 5 %. A deviation of this magnitude shows itself even in the medium slip measured in the successive half-periods.

Table 8—11

Comparison of the medium slip values determined by the graphical procedure and by measurement

Case	Results of the graphical procedure			Measured value
	$\frac{\omega_0 T}{2} = -\int_0^{\pi} \frac{1}{s}\, d\delta$ radian	$\frac{T}{2}$ sec	$s_m = \frac{2}{T}$ %	s_m %
8 MW BO	$2\,\frac{1}{2}\,363360^\circ\,\frac{\pi}{180^\circ} = 6335$	20.2	0.0496	0.0505
12 MW BR	$\frac{2}{1}\,266680^\circ\,\frac{\pi}{180^\circ} = 2333$	7.42	0.1349	0.128
12 MW AO	$\frac{1}{2}\,315310^\circ\,\frac{\pi}{180^\circ} = 2750$	8.75	0.1143	0.111
15 MW AR	$\frac{1}{2}\,\frac{1}{2}\,305909^\circ\,\frac{\pi}{180^\circ} = 1336$	4.25	0.2352	0.243

8.5. *Comparison of the piecewise-linear approximation and the measurement results*

In the forthcoming the results to be obtained by the piecewise-linear approximation and those procured through measurements, as well as obtained by the graphical procedure will be compared for one case : for the asynchro-

nous operation of the turbo-generator with bronze slot-wedges on the rotor and with short-circuited field coil (8 MW BO). As seen in Fig. 8—5, the direct-axis, or quadrature-axis admittance diagram may be well approximated by a single straight section in the range $3\times10^{-4} \leqq s \leqq 8\times10^{-4}$, as this is decisive from the point of view of the 8,1 MW loading.

Starting data (according to Fig. 8—5) :

$$s = 3 \times 10^{-4} \qquad u^2\bar{y}_{q3} = -\ 2.5\ \text{MW} - j\,18.5\ \text{MVAr}$$

$$u^2\bar{y}_{d3} = -\ 7.1\ \text{MW} - j\,18.7\ \text{MVAr}$$

$$s = 8 \times 10^{-4} \qquad u^2\bar{y}_{q8} = -\ 7.8\ \text{MW} - j\,23.0\ \text{MVAr}$$

$$u^2\bar{y}_{d8} = -\ 17.9\ \text{MW} - j\,26.0\ \text{MVAr}.$$

Consequently, the equations of the two linear sections of approximation are:

$$u^2\bar{y}_q = -\ 2.5 - j\,18.5 + (-\ 5.3 - j\,4.5)\ \frac{3 + s\,10^4}{-\ 5}$$

$$u^2\bar{y}_d = -\ 7.1 - j\,18.7 + (-\ 10.8 - j\,7.3)\ \frac{3 + s\,10^4}{-\ 5}.$$

From this, after some rearrangements we obtain :

$$u^2\bar{y}_S = +\ 0.03 - j\,15.06 + (1.61 + j\,1.18)\ s\,10^4$$

$$u^2\bar{y}_D = +\ 0.65 - j\ \ 0.74 - (0.55 + j\,0.28)\ s\,10^4.$$

Consequently, for a loading of

$$-P = -u^2g = 8.1\ \text{MW}$$

formula (5—43) now yields

$$\begin{aligned} -\ 8.1 \ = \ & 0.03 + 1.61\ s\,10^4 \ + \\ & + (0.65 - 0.55\ s\,10^4)\ \cos 2\delta - \\ & - (0.74 - 0.28\ s\,10^4)\ \sin 2\delta. \end{aligned}$$

From this the slip, according to Eq. (5—11) is

$$s(\delta) = 10^{-4}\ \frac{-\ 8.13 - 0.65\cos 2\,\delta + 0.74\sin 2\,\delta}{1.61 - 0.55\cos 2\,\delta - 0.28\sin 2\,\delta}.$$

Fig. 8—25 shows the slip values calculated by the above formula for angles $\delta = 0°,\ 15°,\ 30°,\ \ldots.\ 180°$. In the same figure the related slip and angle values obtained by the graphical procedure may also be seen.

The slip is in form of Eq. (5—22) :

$$s(\delta) = -5.05 \times 10^{-4} \frac{1 - 0.121 \sin(2\delta - 41° 18')}{1 - 0.383 \cos(2\delta - 27°)}$$

while in form of Eq. (5—25) :

$$s'(\delta') = -5.05 \times 10^{-4} \frac{1 - 0.121 \sin 2\delta'}{1 - 0.383 \cos(2\delta' + 14° 18')} .$$

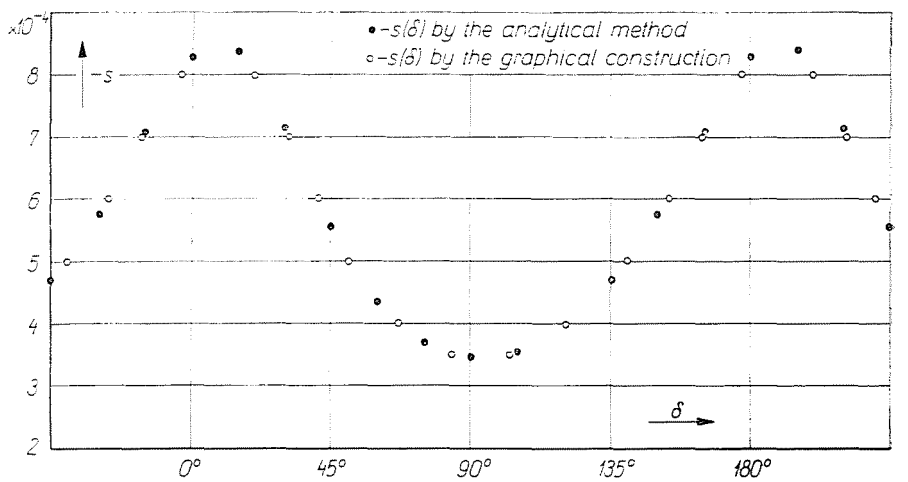

Fig. 8—25

Function $t'(\delta')$ according to Eq. (5—26) is

$$5.05 \times 10^{-4} \times 314\, t' = -0.781\, \delta' + \\ + 1.795 \operatorname{arc\,tg} \frac{0.933 \operatorname{tg} \delta'}{1 - 0.121 \operatorname{tg} \delta'} + \\ + 1.533 \ln(1 - 0.121 \sin 2\delta') .$$

The values of the function $t'(\delta')$ for angles $\delta = 0°,\ 15°,\ 30° \ldots 180°$ are marked by small circles in Fig. 8—26.

It must be noted that knowing the course of $t'(\delta')$ by suitable transposition of the co-ordinate system origin, also the curve $t(\delta)$ is available.

The initial point of curve $t'(\delta')$ has to be removed in the point of abscissa $\delta_0 = 41°18' : 2 = 20°39'$ and ordinate $t_0 = 0.0337\, T$ and by the same two co-ordinates are also the other points of curve $t'(\delta')$ to be displaced to obtain

the curve $t(\delta)$. In Fig. 8—26 standing crosses mark the points of curve $t(\delta)$ originating from the displacement of curve $t'(\delta')$, while the small circles denote the points to be determined by the graphical procedure.

In knowledge of the function $t(\delta)$ on the basis of the relation $s(\delta)$ we have also the function $s(t)$. The small dots in Fig. 8—27 denote the points of the relation $s(t)$ obtained by calculation, while the small circles signify the results of the graphical construction.

Further, according to (5—44) now

$$\begin{aligned} u^2\, b(\delta) \;=\; & 15.06 - 1.18\, s(\delta)\, 10^4 - \\ & - (0.74 + 0.28\, s(\delta)\, 10^4) \cos 2\delta - \\ & - (0.65 - 0.55\, s(\delta)\, 10^4) \sin 2\delta \end{aligned}$$

consequently, substituting $s(\delta)$, $u^2 b$ becomes a function of the angle δ. With this

$$u^2\, y(\delta) = u^2 \sqrt{g^2 + b^2(\delta)} = \sqrt{8.1^2 + u^4 b^2(\delta)}$$

thus, also the apparent power $u^2 y$ is available as function of angle δ.

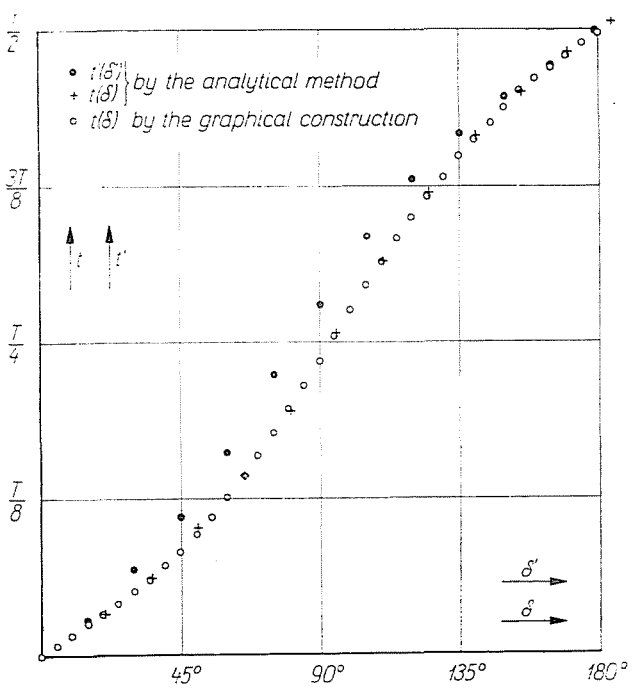

Fig. 8—26

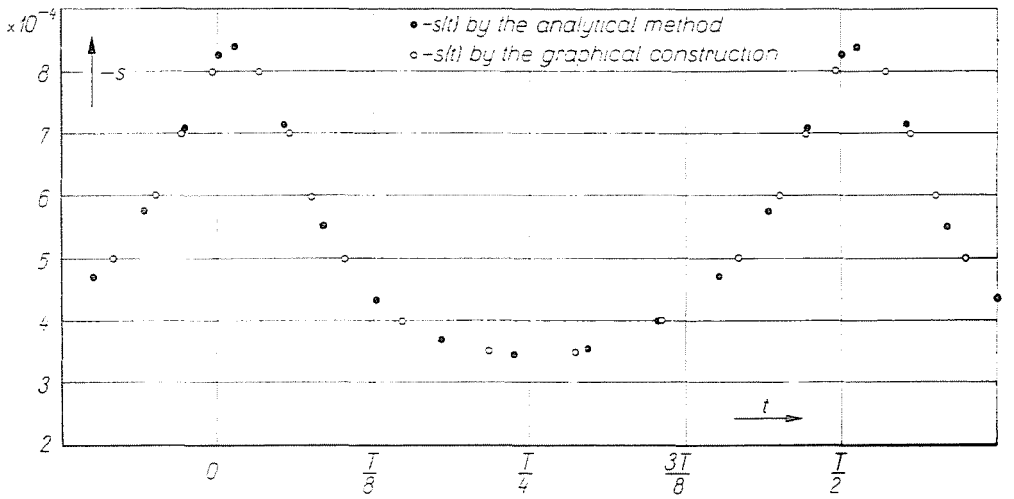

Fig. 8—27

Taking into account the relation $t(\delta)$ from $u^2y(\delta)$ also $u^2y(t)$ may easily be obtained. Fig. 8—28 shows the points of the latter function determined by the above calculation (standing crosses) and by the graphical procedure (small dots), while the full-line curve was plotted on the basis of the oscillograph record.

Finally, according to Eq. (5—28) the medium slip is

$$s'_m = -5.05 \times 10^{-4} \frac{0.0993}{1 + 0.007 \times 0.781} =$$

$$= -4.99 \times 10^{-4} = -0.0499\% .$$

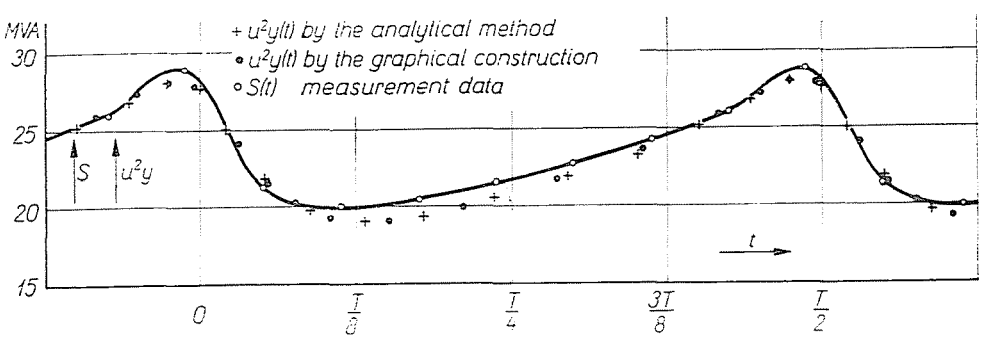

Fig. 8—28

It is worth mentioning that according to Table 8—11 the graphical procedure resulted a medium slip of 0.0496 per cent, while from the measurement the slip is 0.0505 per cent.

8.6. Accuracy of the piecewise-linear approximation

From the previous Fig. 8—28 it may be concluded that through the piecewise-linear approximation in spite of the numerous simplifications and neglections, the time course of the apparent power (stator current) may be determined with a satisfactory accuracy for the practice. Naturally, the final result is considerably influenced by the starting conditions: to what extent we succeeded in approximating the actual admittance diagram.

According to Figs. 8—25 ... 8—28 the piecewise-linear approximation gives practically the same results, as the graphical procedure, when determining the time course of both the angle and slip, as well as of the apparent power (stator current).

8.7. Conclusion

Agreement of the curves determined by the theoretical calculations, or by the graphical constructions and the data of measurements permits to conclude the method suggested in the study (the graphical, as well as the analytical procedure) leading to correct results, further both the starting assumptions and the neglections made admissible. Moreover, the method suggested gives a deep insight into the physical phenomena concerning the asynchronous operation.

As a secondary result of the graphical procedure we succeeded in establishing the section of the direct-axis and quadrature-axis admittance diagrams referring to small slips (*i.e.* to small frequencies), whose determination by other methods would involve great difficulties.

9. Summary of the results

The aim of the study published in four parts (*see* [1, 2, 3] and of the present paper) was to elaborate a practicable engineering method for the determination of the slip, of the stator current and of the apparent and reactive power having a periodic, but not a harmonic course in the asynchronous operation of turbo-generators.

The small value, the "slow" variation, as well as the periodic course of the slip render the three fundamental assumptions acceptable that, on the one hand, the static torque characteristic may be applied and, on the other hand, the torque component arising with angle acceleration due to the inertia

may be neglected, and finally, one may start from the presumption of constant turbine power (or torque).

The terminal point of the resultant admittance vector $\dot{y}$ characteristic of the current (or apparent power) given in expression (3—9) has to pass consequently along the straight line parallel with the imaginary axis, that is, the real part g of $\dot{y}$ given in expression (3—1) must be constant. Relation (3—1) leads to a nonlinear, but separable differential equation, if expression of both the direct-axis and quadrature-axis admittance diagrams are not too complicated. Consequently, on the basis of condition $g = \text{const}$ the slip s as a function of the angle may be determined from (3—1) according to relation (3—2) and then, in accordance with the fundamental relation (3—5) the time t as a function of angle δ may be determined through integral calculus. Finally, knowing the slip-angle $s(\delta)$ and the time-angle $t(\delta)$ functions also the desired slip-time function $s(t)$ is available, while the inverse of the time-angle function $t(\delta)$ provides the wanted angle-time function $\delta(t)$.

Substituting relations $s(t)$ and $\delta(t)$ in expression (3—9) of the resultant admittance, or into its imaginary part, we get the functions

$$\dot{y}(t) \text{ and } b(t)$$

consequently, the course of the apparent power (and the stator current), as well as that of the reactive power (and the reactive current) may be obtained in function of the time.

Success of the method suggested depends on the circumstance, if we succeeded in expressing relation (3—2) in an explicite form and in calculating the left-side integral of (3—5), possibly in a closed form. Realization of both steps is assured by the linear, or quadratic approximation of the direct-axis and quadrature-axis admittance diagrams.

With the *general linear approximation*, *e. g.* the slip-angle function is given in expressions (5—22), or (5—25), while the relation between the angles in Eq. (5—24). The time-angle function may be calculated by formula (5—26), etc.

The same formulae may be adopted in case of *the piecewise-linear approximation*.

In case of the *primitive linear approximation* (the approximate straight line starting from the (negative) imaginary axis and parallel with the (negative) real axis), the slip-angle function is given by Eq. (4—26), while the time-angle function by a somewhat more simple expression (4—28). Study illustrates by a series of figures the time course of the slip and of the angle in case of different parameters β and $\varkappa$, which are defined in Eqs. (4—10) and (4—15). Plotting of a similar series of figures by another analytical method would be extremely laborious.

With the *primitive parabola approximation* (this is the most simple quadratic approximation, the negative imaginary axis being the symmetry axis of the approximating parabolas), the slip-angle function is furnished by expression (6—13), while the time-angle function may be traced back besides elementary integrals to the linear combination of the elliptic integrals of first, second and third kind :

$$F(\varphi, k) \; ; \qquad E(\varphi, k) \; ; \qquad \Pi(\varphi, \alpha^2, k).$$

Besides the *analytic method*, the variation in time of the quantities in question may be determined by *graphical procedure* too. From the points of intersection of the set of circles C_s referring to different slips and furnishing the resultant admittance given by expression (3—9) and of the straight line $g = \text{const}$, the related values δ, s, $\dot{y}$ may be read. The time-angle relation has to be determined according to (3—5) by numerical or graphical integration, thereafter the further steps may be realized without difficulties.

Since the direct-axis and quadrature-axis admittance diagrams necessary for the starting are generally not available, study suggests for construction of the set of circles C_s a simple practical method based on the instrument readings of two series of measurements effected on turbo-generators with a directly short-circuited field and with the field coil closed through the de-excitation resistance.

As a secondary result, the section of the direct-axis and quadrature-axis admittance diagrams referring to small slips (to small frequencies) may be obtained.

Agreement of the curves determined by the method suggested, *i.e.* by the graphical procedure of construction and by the analytic method of calculation, as well as of the oscillograms obtained by measurements for five cases, prove efficiency, practicability and accuracy of the method, as well as competence of the starting assumptions and admissibility of the neglections made.

One may state that the method suggested gives useful means for the explanation, description and clearing of the physical phenomena in connection with the asynchronous operation of turbo-generators.

Summary

Present paper — the fourth and final part of a series consisting of several articles [1, 2, 3] — is divided into three chapters. It suggests, on the one hand, a graphical procedure for plotting the time course of the slip, the stator current, the apparent power, as well as of the reactive power, and, on the other hand, compares the results determined by the graphical and analytical procedure with the oscillograph records. Finally it gives a summary of the main results of the complete study, refers to the formulae of the analytical procedure and to the way to be followed in the course of the graphical procedure.

References

1. CSÁKI, F.: Theoretical Methods Concerned with the Asynchronous Operation of Turbogenerators. Periodica Polytechnica, Electrical Engineering, 1960, 4. N° 2. p. 117.
2. CSÁKI, F.: Linear Approximation of Admittance Diagrams for the Examination of Turbogenerators in Asynchronous Operation. Periodica Polytechnica, Electrical Engineering, 1960, 4. N° 3. p. 145.
3. CSÁKI, F.: Quadratic Approximation of Admittance Diagrams for the Examination of Turbogenerators in Asynchronous Operation. Periodica Polytechnica, Electrical Engineering, 1960, 4. N° 4. p. 259.
4. SEN, S. K.—ADKINS, B.: The Application of the Frequency-Response Method to Electrical Machines. Proceedings of the I.E.E., Part C., May, 1956. Monograph N°. 178. S.

Prof. F. CSÁKI; Budapest XI. Egry József u. 18. Hungary